Supplementary Information (SI) for Inorganic Chemistry Frontiers.
This journal is © the Partner Organisations 2024

Electronic Supplementary Information (ESI)

Defect Engineering of $CH_3NH_3PbI_3$ towards Enhanced Carrier Lifetime: Combined Detailed Balanced Study and NAMD-TDDFT

Jing Wang *[a] and Xiang-Mei Duan [a]

[a] School of Physical Science and Technology, Ningbo University, Ningbo 315211, China

S1. Computational Methods

1.1 First-principles calculations of defect properties

Our first-principles calculations were based on the density functional theory (DFT) as implemented in the Vienna Ab initio Simulation Package (VASP) program.[1, 2] The exchange and correlation interaction were calculated by using the generalized gradient approximation (GGA) with Perdew, Burke, and Ernzerhof (PBE) function[3]. The interaction between the ionic cores and valence electrons was treated by the projector augmented wave (PAW) pseudopotentials[4] with a plane-wave energy cutoff of 400 eV. For the β-$MAPbI_3$ unit cell, its structural optimization for both lattice and atomic coordinates was performed using a Monkhorst-Pack (MP) mesh[5] of 4x4x3 *k*-points in the first Brillouin zone (BZ). The convergence criteria of total energy and force were less than $1x10^{-5}$ eV and 0.01 eV/Å, respectively. The simulated lattice constants were a=8.87 Å and c=13.11 Å, consistent with previous experiment results (a=8.85 Å and c=12.64 Å)[6]. For the defect property calculations, a 2x2x2 supercell with 384-atom was employed to construct the intrinsic defect structures, and the PBE+SOC (spin-orbit coupling) method was used to optimize the global structure (energy and force convergence criteria of $1x10^{-4}$ eV and 0.04 eV/Å, *k*-point using a 1x1x1 gamma mesh). Based on the optimized geometries, we then employed the more accurate hybrid functional calculation with the mixing parameter of 0.36 to obtain a good band gap, and SOC was included. Our HSE+SOC simulation for pristine $MAPbI_3$ supercell yields a band gap of 1.53 eV, agreement with the experimental value of 1.53 eV.[6]

In order to obtain the defect formation energies and charged transition levels, we calculated the total energy $E(\alpha,q)$ for a 2x2x2 supercell containing the relaxed defect α in its charged state q, and total energy $E(MAPbI_3)$ of pristine system with the same size. The defect formation energy is given by the fallowing formula[7-9]:

$$\Delta H_f(\alpha,q) = E(\alpha,q) - E(MAPbI_3) + \sum n_i(\mu_i + E_i) + q(E_{VBM} + E_F + \Delta V) \quad (1)$$

where n_i indicates the atom number of element (i) taken out from pristine supercell to form

the corresponding defect system. μ_i is the chemical potential (CP) of constituent (i), and E_i stands for the total energy of elemental solids of gas at most stable phase. E_{VBM} is the energy of the valence band maximum (VBM) in pristine system, and E_F is the Fermi energy relative to the VBM. ΔV is the correction value for the electronic potential alignment between the supercells with and without the defect.

The defect charged transition energy level (or the thermodynamic ionization level) $\varepsilon(q/q^{'})$ of a defect is defined as E_F position, which satisfies that the formation energy of defect α at the charged state q is equal to that of charged state $q^{'}$, i.e., $\Delta H_f(\alpha,q) = \Delta H_f(\alpha,q^{'})$. This quantity is calculated by applying the general expression:

$$\varepsilon(q/q^{'}) = [E(\alpha,q) - E(\alpha,q^{'})]/(q^{'} - q) \tag{2}$$

1.2 Thermodynamic simulation methods

For any semiconductor system, maintaining the electric neutrality necessitates that total charge of its defect adheres to the condition wherein the sum of positive charges equals the sum of negative charges. This relationship is expressed as[10]:

$$p_0 + \sum_i q_i n_{D_i}^{q_i^+} = n_0 + \sum_j q_j n_{A_j}^{q_j^-} \tag{3}$$

where p_0 and n_0 represent the densities of the thermally excited electrons and holes, respectively, depending on the E_F of system, as elucidated in Equation (3). The terms $\sum_i q_i n_{D_i}^{q_i^+}$ and $\sum_j q_j n_{A_j}^{q_j^-}$ signify the cumulative concentration of various donor defects (n_{D_i}) in their respective positive charge states (q_i^+) and acceptor defect concentration (n_{A_j}) in their respective negative charge states (q_j^-). Meanwhile, these concentrations are influenced by the formation energy of various defect (α) and absolute temperature (T), as depicted in Equation (5). The calculation formulas of these parameters are:

$$p_0 = N_v e^{-\frac{E_F - E_v}{k_B T}}, \qquad n_0 = N_c e^{-\frac{E_c - E_F}{k_B T}}$$

$$N_v = 2\left(\frac{2\pi m_h^* k_B T}{h^2}\right)^{\frac{3}{2}}, N_c = 2\left(\frac{2\pi m_e^* k_B T}{h^2}\right)^{\frac{3}{2}} \tag{4}$$

$$n(\alpha,q) = N_0 e^{-\frac{\Delta H_f}{k_B T}} \quad (5)$$

where N_c and N_v denote the temperature-dependent effective density of conduction band (E_c) and valence band (E_v), respectively. The effective masses of electrons and holes, m_e^* and m_h^*, are specified as m_e^* = 0.18 m_0 and m_h^* = 0.24 m_0 for $MAPbI_3$.[11] The defect concentration $n(\alpha,q)$ can be evaluated by Boltzmann law and calculating the defect formation energy (ΔH_f) through first-principles calculations. N_0 is the density of possible sites for defect α. Through self-consistent solution of the above multiple-equations, we can obtain the E_F, defect concentration, and defect type with maximum defect concentration of semiconductor system at any given CP.

1.3 NAMD simulation methods

To balance the relationship between the computational cost and the reliability of results in NAMD simulation, we adopted 2x2x1 supercell structure. Since β-$MAPbI_3$ is a semiconductor material with a direct energy gap (located at the Gamma point), we use a single *k*-point (1x1x1) for the MD simulation. After re-optimizing the geometry structure (2x2x1, including pristine and defect systems) at 0 K, we perform the Born-Oppenheimer MD simulations using the Nosé thermostat[12, 13] at 300 K, and obtain a 3 ps trajectory with a time step of 1 fs using the canonical ensemble, which is used for the NA coupling calculation. This process uses the Python eXtension for Ab Initio Dynamics (PYXAID)[14, 15] and Quantum Espresso (QE)[16] to calculate NA Hamiltonian. The NAMD simulation is carried out using the semiclassical decoherence-induced surface hopping (DISH) technique.[17] In order to achieve reliable data, we perform the iterative calculations for each NA Hamiltonian to obtain double the Hamiltonian as input data for NAMD simulation. We choose the first half of the double trajectories as the initial condition for calculating the *e*-*h* recombination, and sample the initial condition with 1000 random processes.

S2. Computational details of the coupled kinetic equations

Table S1 summarizes the carrier lifetime of pairwise transitions for perfect and various dominant defect systems by the exponential fitting. The reciprocal of lifetime represents the rate of carrier recombination between pairwise states (described by the symbol *k*), which strongly dependent on the NAC matrix elements d_{ij} between pairwise states, as described by

the following formula[18-20]: $d_{ij} = \frac{\langle \varphi_j | \nabla_R H | \varphi_i \rangle}{\varepsilon_j - \varepsilon_i} \dot{R}$, where H represents the Hamiltonian from the KS equation, φ_i and φ_j are the wave functions of states i and j, ε_i and ε_j are their eigenvalues, and $\dot{R}$ is the nuclear velocity. As can be seen from the formula, the smaller energy gap, stronger electron-phonon coupling, and higher nuclear rate all indicate an increased in the carrier recombination rate. In order to systematically illustrate the total lifetime of excited carriers, it is necessary to consider the whole carrier transition process. Hence, we establish a dynamic model to describe the carrier coupling dynamics of various systems. The detailed description of the carrier recombination/trapping dynamics of these systems is as follows:

(1) For the perfect and resonant defect systems: carrier recombination between electrons in CBM and holes in VBM, as depicted by in the process 1 in Fig. 5a, $\kappa_{(CBM \to VBM)}$.

(2) For systems with defective states inside the bandgap, including shallow- and deep-level defect systems: carrier recombination between electrons in CBM and holes in VBM, as depicted by process 1 in Fig. 5a, $\kappa_{(CBM \to VBM)}$; electrons trapping by defect states (process 2, $\kappa_{(CBM \to trap)}$); recombination of electrons in defect sates with holes in VBM (process 3, $\kappa_{(trap \to VBM)}$); hole trapping by defect states (process 4, $\kappa_{(VBM \to trap)}$);

Thus, the coupled kinetic equations for the perfect and defective systems with the resonant defect states in perovskite $MAPbI_3$ are:

$$\frac{d[VBM]}{dt} = - k_{(CBM \to VBM)}[VBM] \quad (6)$$

$$\frac{d[CBM]}{dt} = \quad k_{(CBM \to VBM)}[CBM] \quad (7)$$

The coupled kinetics equations for V_{MA}^{0} and Pb_{i}^{+1} systems are:

$$\frac{d[VBM]}{dt} = - (k_{(CBM \to VBM)} + k_{(VBM \to trap)})[VBM] \quad (8)$$

$$\frac{d[trap]}{dt} = k_{(VBM \to trap)}[CBM] - k_{(CBM \to trap)})[trap] \quad (9)$$

$$\frac{d[CBM]}{dt} = k_{(CBM \to VBM)}[VBM] + k_{(CBM \to trap)})[trap] \quad (10)$$

The coupled kinetics equations for V_{Pb}^{0}, V_{I}^{0} and I_{i}^{+1} systems are:

$$\frac{d[VBM]}{dt} = - (k_{(CBM \to VBM)} + k_{(CBM \to trap)})[VBM] \quad (11)$$

$$\frac{d[trap]}{dt} = k_{(CBM\to trap)}[CBM] - k_{(trap\to VBM)})[trap] \tag{12}$$

$$\frac{d[CBM]}{dt} = k_{(CBM\to VBM)}[VBM] + k_{(trap\to VBM)})[trap] \tag{13}$$

Where [VBM], [trap] and [CBM] are populations of the VBM, trap and CBM states, respectively. The overall electron lifetime at CBM for all systems are obtained by the exponential fitting, and results are shown in Table S1 and Fig. 5b.

Here, we use the I_i^{+1} defect in perovskite $MAPbI_3$ as an example to describe the carrier relaxation and trapping process (see Table S1 and Fig. 5a). Carrier lifetime or capture rate for the transition of pairwise states is obtained by the DISH method for the two electronic states of interest, and the corresponding fitting results are shown in Fig. S5, S6 and S7.

S3. Supplementary figures and tables

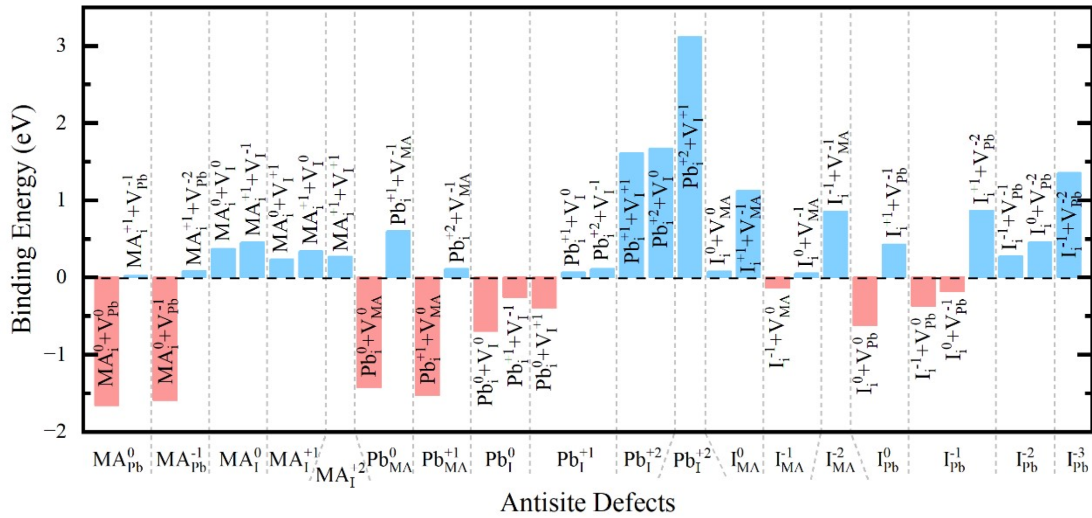

Fig. S1. Defect binding energy of all antisite defects in β-phase $MAPbI_3$.

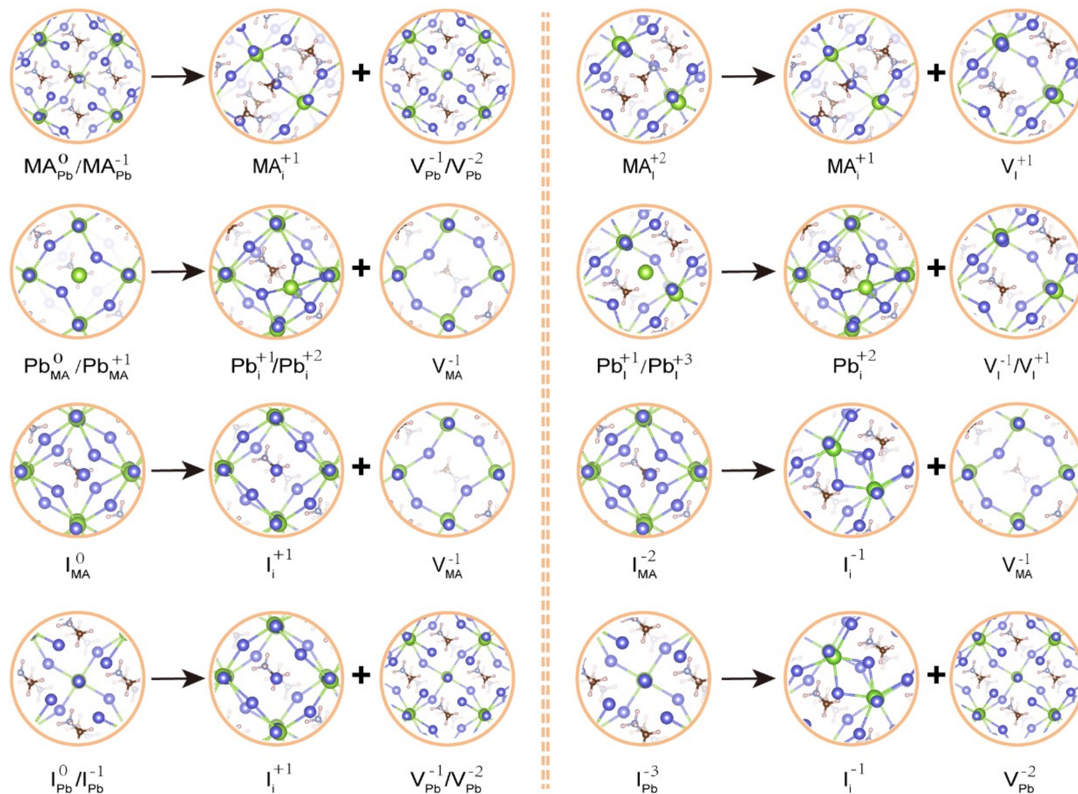

Fig. S2. Evolution process of detailed atomic configuration of the dominant antisite defects in perovskite $MAPbI_3$.

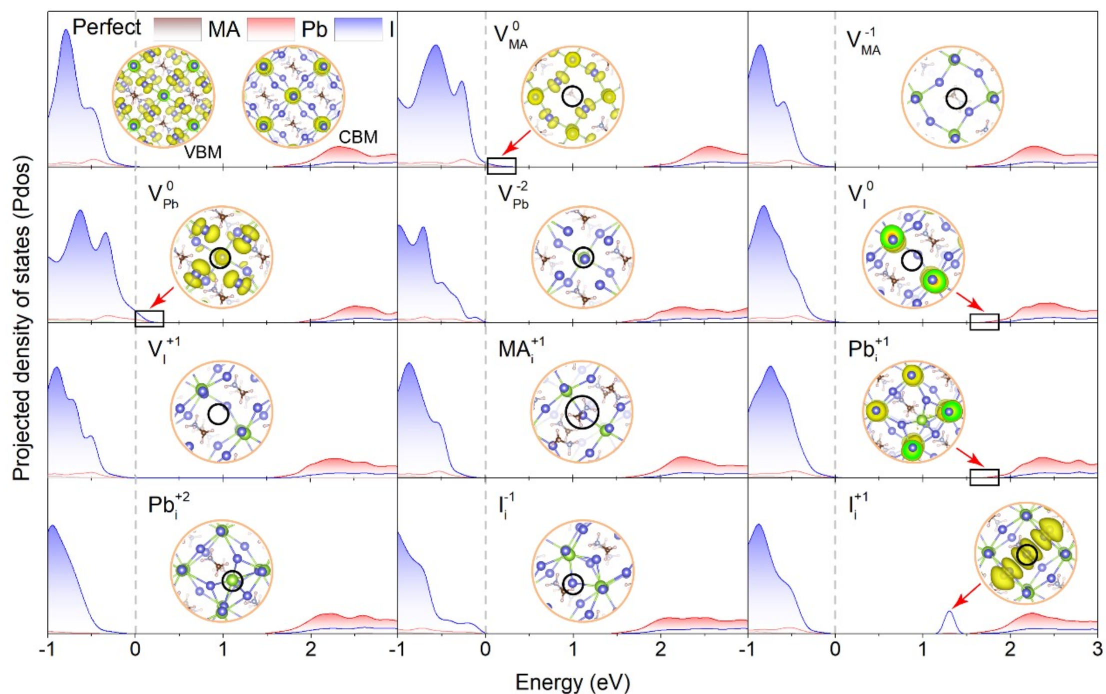

Fig. S3. Projected density of states (PDOS) for pristine $MAPbI_3$ and various defect systems with the different charged states. The energy reference is located at the VBM level. The insets show the charge densities of the band edges in pristine $MAPbI_3$ and the key defect states in defect systems, and the local defect configuration obtained by the optimized geometry. The black

circle indicates the defect position.

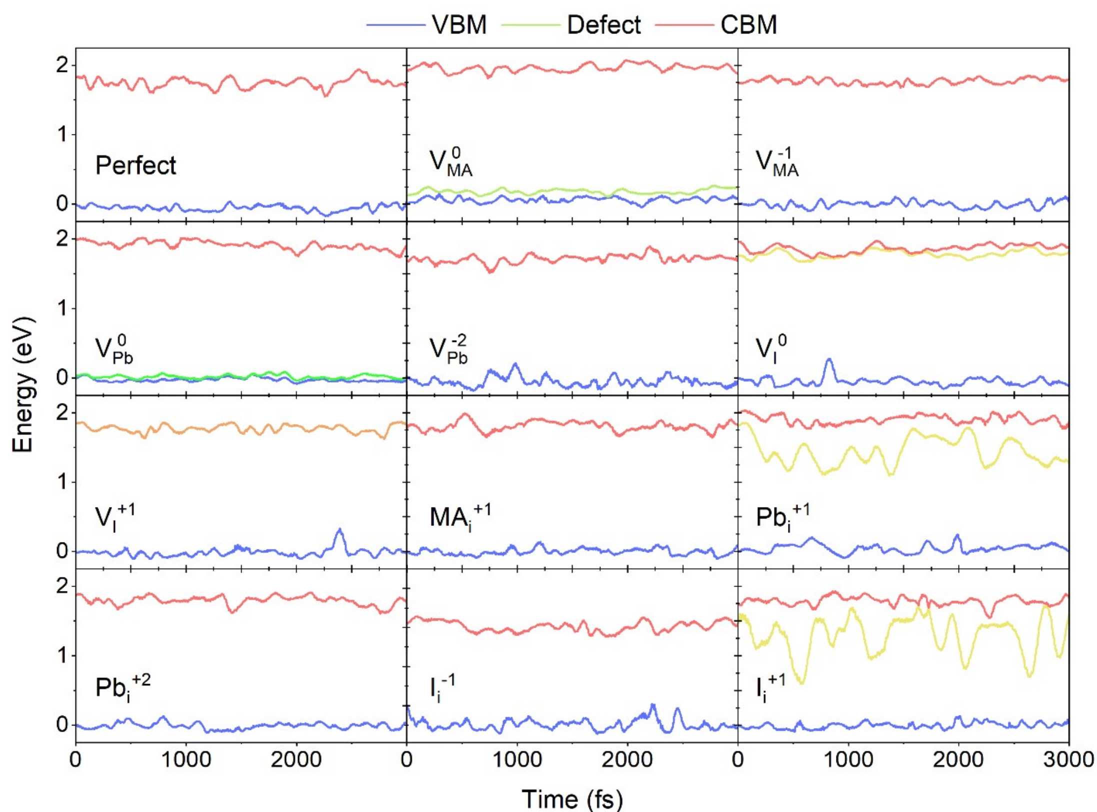

Fig. S4. The time evolution of VBM, CBM and defect states for $MAPbI_3$ system at 300 K.

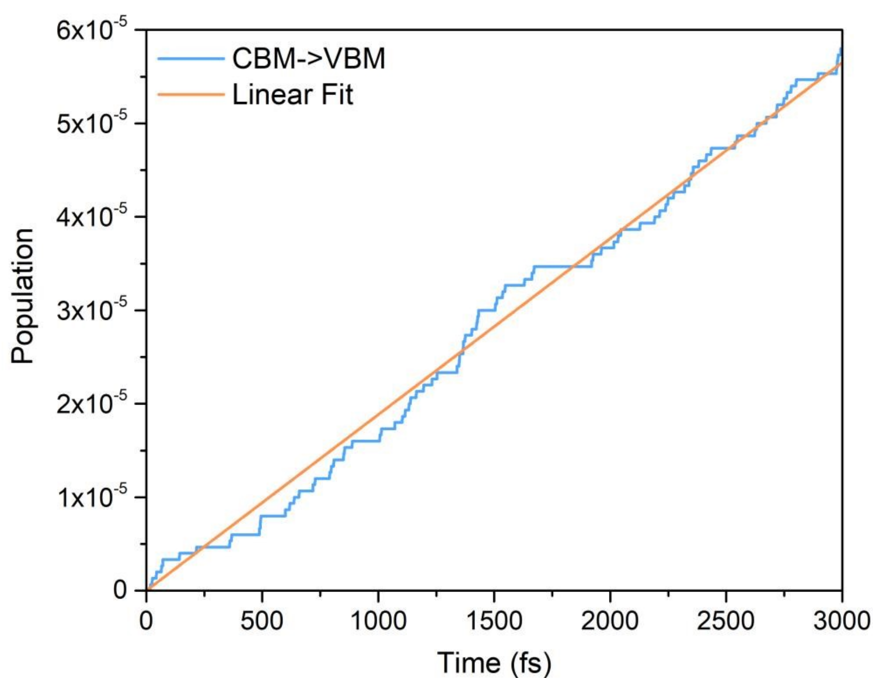

Fig. S5. Population of the CBM state due to relaxation from CBM to VBM in β-$MAPbI_3$ with I_i^{+1} defect. The fitting function is f(t)=t/(53.09x10^6).

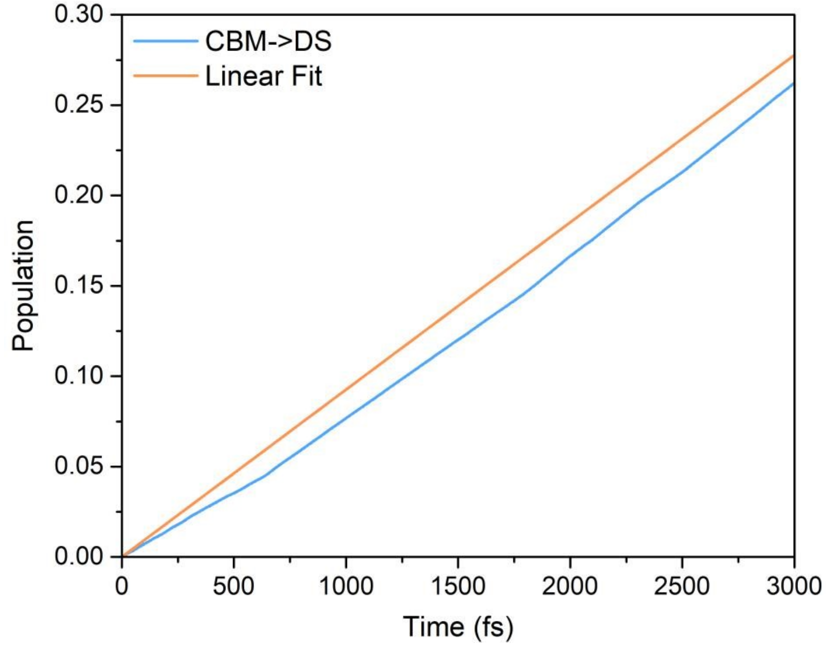

Fig. S6. Population of the defect state (DS) during electron trapping in β-$MAPbI_3$ with the I_i^{+1} defect. The fitting function is f(t)=t/(1.1x10^4).

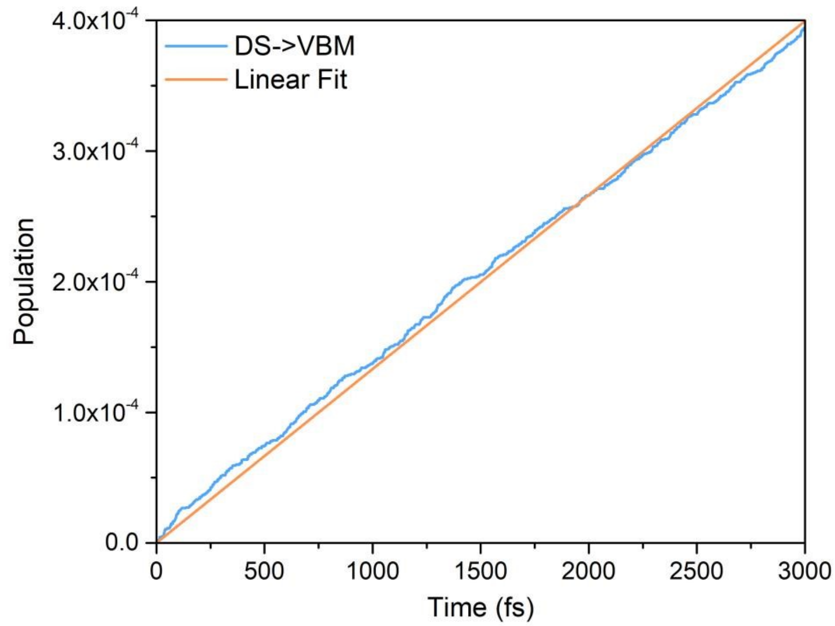

Fig. S7. Population of the defect state (DS) due to recombination of trapped electron with valence band hole in β-$MAPbI_3$ with the I_i^{+1} defect. The fitting function is f(t)=t/(7.51x10^6).

Table S1. Bandgap (eV), Average NA coupling (meV), Nonradiative electrons-hole recombination rate (ns^{-1}), and overall lifetime (ns) for the perfect and various domination

interstitial and vacancy defects in $MAPbI_3$.

		Bandgap (eV)	NA coupling (meV)	Rate constant (ns^{-1})	Overall Lifetime (ns)
Perfect	CBM→VBM	1.53	0.327	0.016	64.29
V_{MA}^{0}	CBM→VBM	1.69	0.337	0.032	40.85
	CBM → Trap	1.46	0.285	0.024	
	VBM → Trap	0.23	3.124	41.667	
V_{MA}^{-1}	CBM→VBM	1.57	0.351	0.021	48.15
V_{Pb}^{0}	CBM→VBM	1.54	0.296	0.018	21.74
	CBM → Trap	1.47	0.356	0.028	
	Trap → VBM	0.07	6.971	227.273	
V_{Pb}^{-2}	CBM→VBM	1.59	0.292	0.021	47.89
V_{I}^{0}	CBM→VBM	1.79	0.315	0.016	35.83
	CBM → Trap	0.30	3.234	45.455	
	Trap → VBM	1.49	0.391	0.028	
V_{I}^{+1}	CBM→VBM	1.59	0.273	0.017	58.36
MA_{i}^{+1}	CBM→VBM	1.57	0.275	0.016	60.79
Pb_{i}^{+1}	CBM→VBM	1.84	0.377	0.024	4.72
	CBM → Trap	0.32	0.896	3.984	
	VBM → Trap	1.52	0.381	0.198	
Pb_{i}^{+2}	CBM→VBM	1.55	0.352	0.023	44.04
I_{i}^{+1}	CBM→VBM	1.56	0.287	0.019	7.52
	CBM → Trap	0.16	2.020	90.909	
	Trap → VBM	1.40	0.292	0.133	
I_{i}^{-1}	CBM→VBM	1.51	0.291	0.018	55.74

Table S2. Reaction energy (E_r) indicates self-healing (non-self-healing) behavior of defect pairs.

Self-healing behaviors		Reaction energy (meV/unit)
Vacancy defects	Interstitial defect	
V_{MA}^{0}	MA_{i}^{0}	-44
V_{MA}^{-1}	MA_{i}^{+1}	-18
V_{Pb}^{0}	Pb_{i}^{0}	-75
V_{Pb}^{-1}	Pb_{i}^{+1}	-43
V_{Pb}^{-2}	Pb_{i}^{+2}	-18
V_{I}^{0}	I_{i}^{0}	-46
V_{I}^{-1}	I_{i}^{+1}	-55
V_{I}^{+1}	I_{i}^{-1}	-24

References

1. G. Kresse and J. Furthmüller, Efficiency of ab-initio total energy calculations for metals and semiconductors using a plane-wave basis set, *Comput. Mater. Sci.,* 1996, **6**, 15-50.
2. G. Kresse and J. Furthmüller, Efficient iterative schemes for ab initio total-energy calculations using a plane-wave basis set, *Phys. Rev. B*, 1996, **54**, 11169.
3. J. P. Perdew, K. Burke and M. Ernzerhof, Generalized gradient approximation made simple, *Phys. Rev. Lett.,* 1996, **77**, 3865.
4. G. Kresse and D. Joubert, From ultrasoft pseudopotentials to the projector augmented-wave method, *Phys. Rev. B*, 1999, **59**, 1758.
5. H. J. Monkhorst and J. D. Pack, Special points for Brillouin-zone integrations, *Phys. Rev. B*, 1976, **13**, 5188.
6. C. C. Stoumpos, C. D. Malliakas and M. G. Kanatzidis, Semiconducting tin and lead iodide perovskites with organic cations: phase transitions, high mobilities, and near-infrared photoluminescent properties, *Inorg. Chem.*, 2013, **52**, 9019-9038.
7. C. G. Van de Walle and J. Neugebauer, First-principles calculations for defects and impurities: Applications to III-nitrides, *J. Appl. Phys.,* 2004, **95**, 3851-3879.
8. H.-P. Komsa, T. T. Rantala and A. Pasquarello, Finite-size supercell correction schemes for charged defect calculations, *Phys. Rev. B*, 2012, **86**, 045112.
9. S. Lany and A. Zunger, Assessment of correction methods for the band-gap problem and for finite-size effects in supercell defect calculations: Case studies for ZnO and GaAs, *Phys. Rev. B,* 2008, **78**, 235104.
10. J.-H. Yang, W.-J. Yin, J.-S. Park, J. Ma and S.-H. Wei, Review on first-principles study of defect properties of CdTe as a solar cell absorber, *Semi. Sci. Technol.*, 2016, **31**, 083002.
11. P. Umari, E. Mosconi and F. De Angelis, Relativistic GW calculations on CH3NH3PbI3 and CH3NH3SnI3 perovskites for solar cell applications, *Sci. Rep.*, 2014, **4**, 4467.
12. S. Nosé, A unified formulation of the constant temperature molecular dynamics methods, *J. Chem. Phys.,* 1984, **81**, 511-519.
13. N. Shuichi, Constant temperature molecular dynamics methods, *Prog. Theor. Phys. Suppl.* 1991, **103**, 1-46.
14. A. V. Akimov and O. V. Prezhdo, Advanced capabilities of the PYXAID program: integration schemes, decoherence effects, multiexcitonic states, and field-matter interaction, *J. Chem. Theory Comput.*, 2014, **10**, 789-804.
15. A. V. Akimov and O. V. Prezhdo, The PYXAID program for non-adiabatic molecular dynamics in condensed matter systems, *J. Chem. Theory Comput.*, 2013, **9**, 4959-4972.
16. P. Giannozzi, S. Baroni, N. Bonini, M. Calandra, R. Car, C. Cavazzoni, D. Ceresoli, G. L. Chiarotti, M. Cococcioni and I. Dabo, QUANTUM ESPRESSO: a modular and open-source software project for quantum simulations of materials, *J. Phys.: Condens.Matter*, 2009, **21**, 395502.
17. H. M. Jaeger, S. Fischer and O. V. Prezhdo, Decoherence-induced surface hopping, *J. Chem. Phys.,* 2012, **137**, 22A545.
18. J. He, W-H Fang and R. Long, Unravelling the effects of oxidation state of interstitial iodine and oxygen passivation on charge trapping and recombination in $CH_3NH_3PbI_3$ perovskite: a time-domain ab initio study, *Chem. Sci.*, 2019, **10**, 10079.
19. W. Chu, Q. Zheng, O. V. Prezhdo, J. Zhao and W. A. Saidi, Low-frequency lattice phonons in halide perovskites explain high defect tolerance toward electron-hole recombination. *Sci. Adv.*, 2020, **6**, eaaw7453

20. W. Chu, W. A. Saidi, J. Zhao and O. V. Prezhdo, Soft Lattice and Defect Covalency Rationalize Tolerance of β-$CsPbI_3$ Perovskite Solar Cells to Native Defects, *Angew. Chem., Int. Ed.*, 2020, 59, 6435.